



Robust Design of 3D-Printed W-Band Bandpass Filters Using Gap Waveguide Technology

David Santiago¹ · Adrián Tamayo-Domínguez² · Miguel A. G. Laso¹ · Txema Lopetegui¹ · José-Manuel Fernández-González² · Ramón Martínez² · Iván Arregui¹

Received: 18 October 2022 / Accepted: 26 December 2022
© The Author(s) 2022

Abstract

In this paper, a W-band 3D-printed bandpass filter is proposed. The use of higher-order TE_{10n} modes in groove gap waveguide (GGW) technology is evaluated in order to alleviate the manufacturing requirements. In addition to the use of higher-order modes, the coupling between them is analyzed in detail to improve the overall fabrication robustness of the component. This allows the implementation of narrow-band filters operating at millimeter-wave frequency bands (or above), which usually demand complex manufacturing techniques to provide the high accuracy required for this kind of devices. In order to show the applicability of the proposed method, a narrow-band 5th-order Chebyshev bandpass filter centered at 94 GHz, which can be easily fabricated by state-of-the-art stereolithographic (SLA) 3D-printing techniques followed by silver coating, is shown. Excellent measured performance has been obtained.

Keywords Bandpass filter · Groove gap waveguide · W-band · 3D-printing

1 Introduction

Millimeter-wave frequency bands are used nowadays in radar and communication systems to increase their capacity and data rate. However, the implementation of high-performance filters becomes challenging at these frequencies due to the manufacturing imperfections associated to the small dimensions required. For instance,

✉ David Santiago
david.santiago@unavarra.es

¹ Institute of Smart Cities (ISC), Department of Electrical, Electronic and Communications Engineering, Public University of Navarre (UPNA), Pamplona, Spain

² Radiation Group, Department of Signals, Systems and Radiocommunications, Information Processing and Telecommunications Center (IPTC), Universidad Politécnica de Madrid, Madrid, Spain

rectangular waveguide technology is typically employed in applications where low loss is a requirement and some issues, such as a perfect alignment and contact between the different waveguide parts, become difficult at millimeter waves. In order to overcome these practical drawbacks, the use of the groove gap waveguide (GGW) technology was proposed [1–4], see Fig. 1, giving more manufacturing robustness compared to other waveguides such as rectangular waveguide. At lower frequencies, GGW technology has also been used where having a contactless geometry provides a useful advantage, for instance, to design moveable structures [5]. This technology is based on two parallel metal plates where one of them has a metal pin bed that introduces a high impedance condition at the plane over the pins. This allows the top metal plate to be placed at any distance from the top of the pins, provided that this distance is smaller than $\lambda/4$, and any alignment and contact requirements are avoided [6].

Complex manufacturing methods such as laser micromachining, deep reactive ion etching, or SU-8 processes can be used to fabricate millimeter-wave filters [7]. However, computer numerical control (CNC) milling is still the most commonly employed method in industry due to its simplicity and long tradition within the space and cellular communication base-station sectors, for instance.

Unfortunately, the fabrication tolerance that low-cost CNC milling provides could not be enough at millimeter-waves. Recently, other simple additive manufacturing technologies, such as the stereolithographic (SLA) 3D-printing method, have emerged and are rapidly evolving, being a promising alternative to CNC milling in some applications and benefiting from the inherent general advantages of 3D-printing for RF components [8]. SLA 3D-printing is especially suitable to fabricate GGW devices, since it allows the implementation of a large number of pins (if required) without increasing the time or cost of the process (unlike CNC milling) [9]. This approach has been employed in [10] to implement Ka-band (35.5 GHz) bandpass filters (BPFs) based on $\lambda/2$ cavities.

In this paper, a W-band (94 GHz) BPF is shown using SLA 3D-printing GGW technology for the first time. At this frequency, $\lambda/2$ cavities fail to provide enough fabrication robustness and the behavior of the cavities with respect to fabrication tolerances must be improved. The use of higher-order resonant modes is proposed allowing us to work with cavities of larger dimensions where the inter-cavity couplings remain also more resistant to manufacturing imperfections. The design method will be explained in

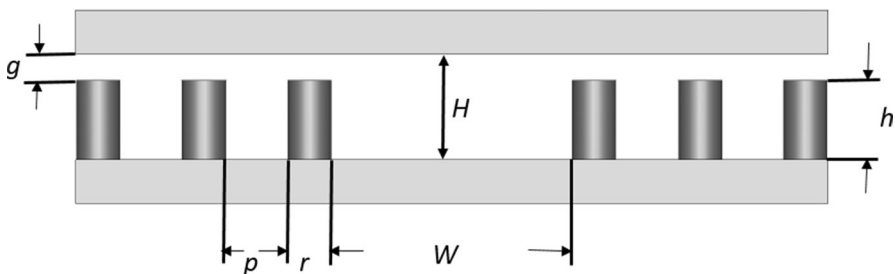


Fig. 1 Section of a GGW including the base with the pin bed and the top plate

Section 2, a design example including a prototype and comparisons with other state-of-the-art filters will be given in Section 3, and some final conclusions will be highlighted at the end of the paper.

2 Design Method

The bandpass filters proposed in this paper feature the coupling mechanism shown in Fig. 2, where S and L stand for the source and the load excitation, Q_{ext} represents the external quality factor, R_i corresponds to each resonator of the structure, and $k_{i,i+1}$ is the coupling coefficient between resonators. The resonant frequency, $f_{0,pqn}$, of the TE_{pqn} modes can be estimated as in [11]:

$$f_{0,pqn} = \frac{c}{2\pi} \sqrt{\left(\frac{p\pi}{W}\right)^2 + \left(\frac{q\pi}{H}\right)^2 + \left(\frac{n\pi}{l}\right)^2} \tag{1}$$

where c is the speed of light in free-space and W , H , and l are the width, height, and length of the resonator, respectively. Moreover, the external quality factor and the coupling coefficients can be calculated by the following equations [11]:

$$K_{i,i+1} = \frac{BW}{\sqrt{g_i \cdot g_{i+1}}}, i = 1, \dots, N - 1 \tag{2}$$

$$Q_{ext} = \frac{g_i \cdot g_{i+1}}{BW}, i = 0, N \tag{3}$$

where g_i are the normalized coefficients of the corresponding low-pass prototype. The frequency behavior of this kind of BPFs based on coupled resonators is determined by the resonant mode as well as the coupling geometry. Higher-order modes are typically avoided since they may lead to bulky structures with spurious responses [10]. However, they can be also very useful to facilitate the fabrication process of rectangular waveguide components at very high frequencies and improve the insertion loss of the filter, such as in [12], where the TM_{120} mode was used or in [13], and where the TE_{102} was employed for this purpose.

In this section, the behavior of the TE_{10n} modes is analyzed to select a suitable mode for the implementation of GGW BPFs at millimeter-waves. As previously suggested [12, 13], it is well known that the use of larger cavities (higher values of n) will reduce the deviation of the resonant frequency of these cavities when manufacturing imperfections occur. Additionally, it is also interesting to analyze the coupling, $k_{i,i+1}$, between two adjacent GGW cavities when the TE_{10n} modes are used. In this paper, $k_{i,i+1}$ (obtained as explained in [11]) represents the coupling between the i -th and

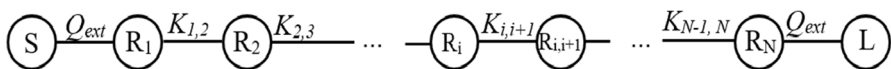


Fig. 2 Coupling mechanism of the proposed structure

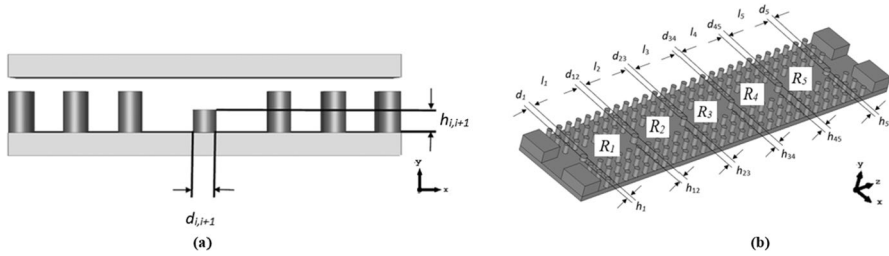


Fig. 3 Schematic of a BPF implemented in GGW. **(a)** Front view of the filter at the waveguide port. **(b)** General view of the filter with the top plate removed

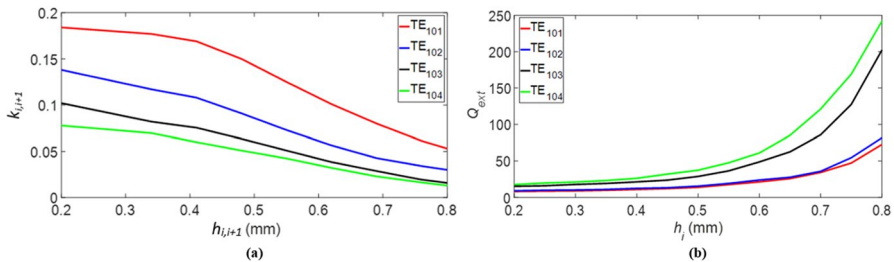


Fig. 4 Comparison of the behavior of the TE_{10n} modes ($n=1, 2, 3, 4$) using GGW technology ($W=2.75$ mm, $H=1.2$ mm, $g=0.3$ mm, $h=0.9$ mm, $r=0.5$ mm, and $p=0.7$ mm) and $d_i=d_{i,i+1}=0.6$ mm. **(a)** Coupling coefficient, $k_{i,i+1}$, between two adjacent cavities. **(b)** External quality factor, Q_{ext}

$i + 1$ -th cavities when they are separated by a simple cylindrical post of $h_{i,i+1}$ height (see Fig. 3). This parameter is evaluated in Fig. 4a, where $k_{i,i+1}$ is shown for different modes as a function of $h_{i,i+1}$. As expected, as $h_{i,i+1}$ changes, the coupling coefficient between the i -th and $i + 1$ -th cavities also varies for all the TE_{10n} modes. Moreover, it can be noticed that employing a cylindrical post as coupling structure, it is only possible to achieve the small values of $k_{i,i+1}$ that are required to design narrow-band BPFs with the higher-order modes (higher n). It can be also seen in Fig. 4a that the variation of $k_{i,i+1}$ vs. $h_{i,i+1}$ is smoother for the higher-order modes, which is convenient to reinforce the fabrication robustness. If other coupling structures are used, different values would be achieved, but the same trends and conclusions would be obtained.

Equivalent conclusions can be also drawn by analyzing the external quality factor, Q_{ext} , which controls the signal input/output coupling of the first/last cavity. It can be observed in Fig. 4b that, as n increases, it is possible to achieve the high Q_{ext} values that are sometimes required in the design of narrow-band filters. Moreover, it is interesting to note that, given a fixed Q_{ext} , a smaller ΔQ_{ext} deviation is achieved for a fixed Δh_p , being h_i the height of the post in the first/last cavity.

For instance, if $Q_{ext} = 25$ and h_i is varied ± 50 μm , i.e., $\Delta h_i = 100$ μm , then, $\Delta Q_{ext} = 13.03$ for the TE_{101} , 11.92 for the TE_{102} , 7.47 for the TE_{103} , and 5.17 for the TE_{104} modes. Again, the higher the n , the more robust the filter is to manufacturing imperfections. However, the filter size also increases. The TE_{103} mode offers a good trade-off in our case and will be used in Section 3. The TE_{103} mode will resonate in

$3\lambda/2$ -long cavities and, as above, simple cylindrical posts will be employed to control the coupling between the cavities. In practice, h_i and $h_{i,i+1}$ will be a multiple of l_r , being l_r the 3D-printing layer resolution. In order to finely adjust the required coupling, the diameter of the posts can be modified, since there are not manufacturing constrains for this parameter in the xz -plane (Fig. 3).

3 Design Example

As a design example, a filter to be integrated with the 94 GHz monopulse radar antenna proposed in [14] and [15] will be implemented. Specifically, a narrow-band BPF centered at 94 GHz will be designed and manufactured. It is important to highlight that, unlike in this paper, such a filter with very narrow bandwidth would generally lead to devices with a large insertion loss and low robustness against manufacturing errors, which could not be fabricated by low-cost techniques such as SLA 3D-printing.

3.1 Design and Simulation

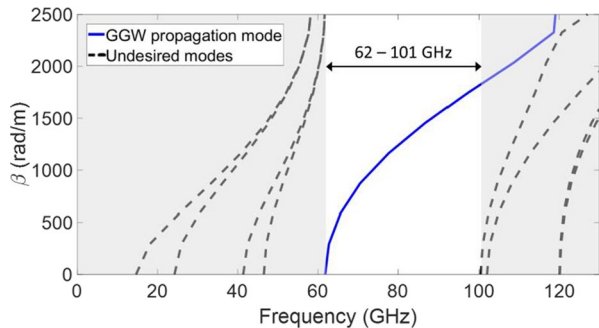
In order to design a filter in GGW technology, the following dimensions (shown in Fig. 1) will be employed: $W = 2.75$ mm, $H = 1.2$ mm, $g = 0.3$ mm, $h = 0.9$ mm, $r = 0.5$ mm, and $p = 0.7$ mm. This allows us to work between 62 and 101 GHz in single-mode configuration (Fig. 5).

As detailed in [16], an estimation of the insertion loss parameter of a filter can be obtained using Eq. (4):

$$I_L(\text{dB}) = \frac{4,343 \cdot f_0}{\Delta f \cdot Q_u} \sum_{i=1}^N g_i \tag{4}$$

f_0 being the central frequency, Δf the bandwidth of the passband, and Q_u the unladen quality factor. The central frequency, f_0 , is fixed by the application and, according to (4), high-order filters or very narrow bandwidths lead to filters that may become too lossy. Therefore, a 5th-order Chebyshev BPF centered at $f_0=94$ GHz with a bandwidth $\Delta f=3$ GHz and 20 dB of return loss is designed ($g_0=g_6=1$,

Fig. 5 Dispersion diagram of the GGW employed



$g_1 = g_5 = 0.9732$, $g_2 = g_4 = 1.3723$, and $g_3 = 1.8032$). The use of high-order TE_{10n} modes, as mentioned previously, will provide us with large Q_u resonators, as well as a robust structure for fabrication. Specifically, the Q_u value of the TE_{103} -mode GGW resonators obtained by the CST MWS Eigenmode Solver (considering $f_0 = 94$ GHz and the ideal conductivity of silver $6.3012 \cdot 10^7$ S/m) is $Q_u = 3313$. This results in an estimated insertion loss equal to 0.27 dB. By using the design parameters in Eqs. (2) and (3), the following Q_{ext} and $k_{i,i+1}$ values can be obtained: $Q_{ext} = 41.85$, $k_{12} = k_{45} = 0.0276$, and $k_{23} = k_{34} = 0.0203$. Considering that the TE_{103} mode has been selected as the resonant mode of the filter cavities, Fig. 4 (black line) can be used to determine the heights of the cylindrical posts h_i and $h_{i,i+1}$. As explained previously, h_i and $h_{i,i+1}$ must be a multiple of the layer resolution, $l_r = 50$ μm in this case. The diameter of the posts, d_i and $d_{i,i+1}$, can be used to slightly adjust the specific value of the required coupling coefficients. The final dimensions are shown in Table 1 along with the length of the resonators, l_i , the latter also after slight optimization.

In order to analyze the robustness of the structure against fabrication errors, a yield analysis has been carried out. Specifically, the main dimensions of the device, i.e., the height, diameter, and position of the posts, which determine the frequency response of the filter, have been varied. Considering the tolerance values provided by the manufacturer (± 130 μm in the z -axis and ± 50 μm in the x - and y -axis), these dimensions have been modified accordingly. By means of the post-processing tool of CST MWS, the yield results shown in Table 2 have been obtained. As it can be seen in this table, 15 dB has been employed as the target return loss while two different bandwidths have been considered: 3 GHz (design bandwidth) and 0.5 GHz (bandwidth of special interest around the central frequency of 94 GHz). For instance, varying the height of the posts, h_i , can lead to

Table 1 Final dimensions of the design example

Symbol	Value (mm)
l_1	5.58
l_2	5.48
l_3	5.59
l_4	5.48
l_5	5.58
h_1	0.40
h_5	0.40
h_{12}	0.70
h_{23}	0.75
h_{34}	0.75
h_{45}	0.70
d_1	0.73
d_5	0.73
d_{12}	0.70
d_{23}	0.53
d_{34}	0.53
d_{45}	0.70

Table 2 Manufacturing yield analysis of the proposed device

Parameter	BW (GHz)	RL bound (dB)	Manufacturing tolerance (μm)	Manufacturing yield (%)
Height of the posts	3	15	130	53.55
Post position	3	15	50	54.31
Diameter of the posts	3	15	50	66.05
Height, diameter, and post position	3	15	130/50/50	53
Height of the posts	0.5	15	130	64.95
Post position	0.5	15	50	58.5
Diameter of the posts	0.5	15	50	100
Height, diameter, and post position	0.5	15	130/50/50	57.56

the poorest manufacturing yield (still 53.55% though) for the 3 GHz bandwidth, but it is worth noting that, in this case, h_i would suffer a deviation of $\pm 130 \mu\text{m}$ (a dramatic change considering the operation frequency), proving the robustness of our design. Moreover, when all the dimensions are modified at the same time, values larger than 50 % are obtaining for both bandwidths, again showing that even at very extreme cases where all fabrication errors are against a good performance, the design is robust enough to reasonably expect good results at 94 GHz.

Moreover, in order to facilitate the connection of the device with the measurement setup as well as its final integration with the monopulse antenna [14], the GGW to WR-10 ($2.54 \times 1.27 \text{ mm}$) transitions considered also in [14] have been included, as depicted in Fig. 6. The simulated frequency response of the design example—using CST Microwave Studio (MWS)—is shown in Fig. 7 (gray line), using the conductivity of silver ($6.3012 \cdot 10^7 \text{ S/m}$) for the base with the pin bed and aluminum ($3.56 \cdot 10^7 \text{ S/m}$) for the top plate. Moreover, a surface roughness equal to $0.2 \mu\text{m}$ has been considered.

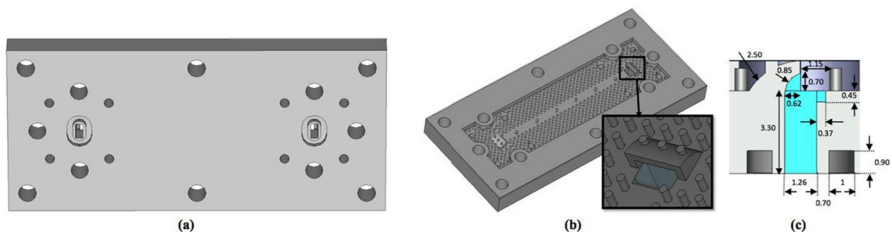


Fig. 6 Designed BPF including GGW to WR-10 transitions. **(a)** Top view of the device (with the top-plate removed). **(b)** Bottom view showing the waveguide excitation ports. **(c)** Internal dimensions of the transition to WR-10

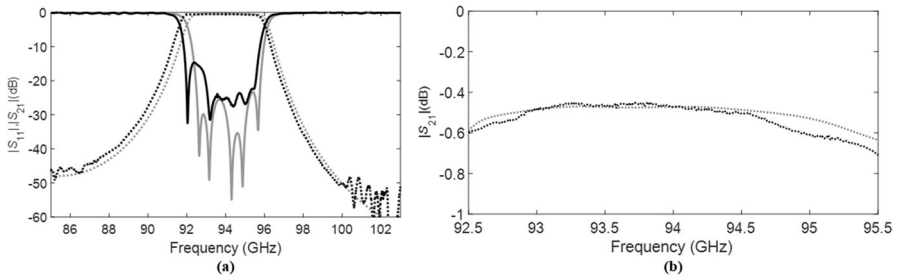


Fig. 7 CST MWS simulated frequency response of the BPF including the GGW to WR-10 transitions (gray line) and measured response of the fabricated prototype (black line). (a) $|S_{11}|$ in solid line and $|S_{21}|$ in dashed line. (b) Detail of the insertion loss

3.2 Fabrication and Measurement

The base with the pin bed of the filter has been fabricated by SLA 3D-printing and then coated with 10 μm of silver. An aluminum sheet is included over the pin bed as the filter top plate. A photograph of the prototype is given in Fig. 8 and the corresponding measured frequency response in Fig. 7 (black line). The excellent performance at 94 GHz shows the feasibility of robust designs of BPFs in GGW at millimeter-waves using low-cost SLA 3D-printing.

3.3 Literature Comparison

As detailed in Table 3, most of the devices previously proposed in W-band aimed for wider passbands, which facilitated the fabrication process. This is the case of the structures presented in [12, 17, 19, 20], where the filters have been implemented in rectangular waveguide. Good results can be achieved with devices fabricated by CNC milling and also by SLA 3D-printing, when wide passbands are considered.

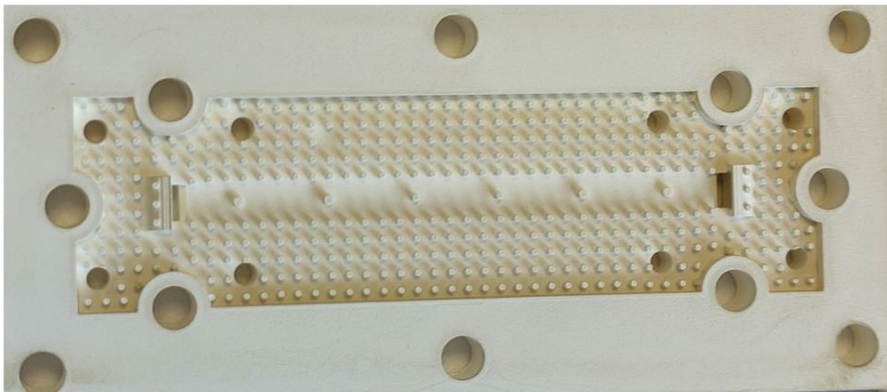


Fig. 8 Photograph of the fabricated prototype with the top plate removed

Table 3 Comparison of the proposed filter with previous works

Ref	Technology	Manufactured technique	Order	Insertion loss (dB)	Return loss (dB)	f_0 (GHz)	Fractional bandwidth (%)
[12]	Rectangular waveguide	CNC milling	4	0.5 (average level)	> 13 (worst level)	100	6
[17]	Rectangular waveguide	CNC milling	5	0.6 (average level)	> 15 (worst level)	92.5	20.2
[19]	Rectangular waveguide	SLA	4	0.26–0.48 (best to worst level)	> 17 (worst level)	101.14	11.10
[20]	Rectangular waveguide	SLA	4	0.3–0.5 (best to worst level)	> 18 (worst level)	87.5	11.5
[18]	GGW	CNC milling	3	1 (average level)	> 9 (worst level)	35	1
[10]	GGW	SLA	4	0.5 (center frequency)	21 (central frequency)	35.65	1.4
[21]	GGW	DRIE	4	0.9–1.6 (best to worst level)	> 15 (worst level)	93.6	8
This work	GGW	SLA	5	0.45–0.61 (best to worst level) 0.466 (central frequency)	> 15 (worst level) 25.2 (central frequency)	94	3.2

When the fabrication requirements are alleviated by the use of GGW technology, very good frequency behaviors have been also achieved for narrow bandwidths in devices fabricated by milling [18] or SLA 3D-printing [10]. However, it is important to note that these results have been achieved at frequencies around 35 GHz (vs. 94 GHz in this work). Working at higher frequencies and with narrow bandwidths require to re-think the design process as we have done in this paper. In order to use the GGW technology to design filters operating at W-band, the complex and expensive deep reactive ion etching (DRIE) method has been also proposed in [21], where a compact device is obtained but with a large insertion loss. By means of the design procedure previously explained, a filter with better insertion loss levels has been obtained, which can be fabricated at W-band by using a simple, commercially-available, and low-cost SLA 3D-printing technique.

4 Conclusion

A GGW BPF operating at 94 GHz and fabricated by SLA 3D-printing has been proposed for the first time and excellent measured results have been obtained. On the one hand, the intrinsic attributes of the GGW technology contributed to the manufacturing robustness and, on the other hand, a higher-order TE_{103} resonant mode helped to achieve simpler geometries easily fabricated by SLA 3D-printing. This seems a promising approach for 3D-printed filters at millimeter waves.

Author Contributions David Santiago wrote the main manuscript text. Adrián Tamayo prepared figures 7-8 and David Santiago prepared figures 1-6 and tables 1-2. All authors reviewed the manuscript.

Funding Open Access funding provided by Universidad Pública de Navarra. This work was funded by the Spanish Ministerio de Ciencia e Innovación –Agencia Estatal de Investigación (MCIN/AEI/1010.13039/501100011033) under Projects TEC2017-85529-C3-1-R and TEC2017-85529-C3-2-R (co-funded by FEDER “A way to make Europe”) and Projects PID2020-112545RB-C51 and PID2020-112545RB-C53.

Data Availability There are no supplementary materials, and the data is available upon reasonable request.

Declarations

Competing Interests The authors declare no competing interests.

Conflict of Interest The authors declare no competing interests.

Open Access This article is licensed under a Creative Commons Attribution 4.0 International License, which permits use, sharing, adaptation, distribution and reproduction in any medium or format, as long as you give appropriate credit to the original author(s) and the source, provide a link to the Creative Commons licence, and indicate if changes were made. The images or other third party material in this article are included in the article's Creative Commons licence, unless indicated otherwise in a credit line to the material. If material is not included in the article's Creative Commons licence and your intended use is not permitted by statutory regulation or exceeds the permitted use, you will need to obtain permission directly from the copyright holder. To view a copy of this licence, visit <http://creativecommons.org/licenses/by/4.0/>.

References

1. P. -S. Kildal, E. Alfonso, A. Valero-Nogueira, and E. Rajo-Iglesias. "Local metamaterial-based waveguides in gaps between parallel metal plates." *IEEE Antennas and Wireless Propagation Letters*, 8 84, 2009. <https://doi.org/10.1109/LAWP.2008.2011147>.
2. P.-S. Kildal. "Waveguides and transmission lines in gaps between parallel conducting surfaces". European patent application EP08159791.6, 2008. <https://patents.google.com/patent/US20110181373A1/en>.
3. E. A. Alós, A. U. Zaman and P. -S. Kildal, "Ka-Band gap waveguide coupled-resonator filter for radio link diplexer application". *IEEE Transactions on Components, Packaging and Manufacturing Technology*, 3(5), pp. 870-879, 2013, <https://doi.org/10.1109/TCPMT.2012.2231140>.
4. E. Puzzi, A. U. Zaman, E. Rajo-Iglesias, P. Kildal, and A.Kishk. "Study of Q-factors of ridge and groove gap waveguide resonators". *IEEE Transactions on Microwave Theory and Techniques*, 7(11), pp. 900-908, 2003. <https://doi.org/10.1049/iet-map.2013.0081>.
5. J. Tayebpour, B. Ahmadi, M. Fallahzadeh, O. Shekoofa, and A. Torabi. "A waveguide switch based on contactless gap waveguide technology". *IEEE Microwave and Wireless Components Letters*, 29 12 771-774, 2019. <https://doi.org/10.1109/LMWC.2019.2950164>.
6. A. Berenguer, V. Fusco, D. E. Zelenchuk, D. Sánchez-Escuderos, M. Baquero-Escudero, and V. E. Boria-Esbert. "Propagation characteristics of groove gap waveguide below and above cutoff". *IEEE Transactions on Microwave Theory and Techniques*, 64(1), pp. 27-36, 2016. <https://doi.org/10.1109/TMTT.2015.2504501>.
7. R. V. Snyder, G. Macchiarella, S. Bastioli, and C. Tomassoni. "Emerging trends in techniques and technology as applied to filter design." *IEEE Journal of Microwaves 1*, no. 1 (2021): 317-344. <https://doi.org/10.1109/JMW.2020.3028643>.
8. C. Tomassoni, O. A. Peverini, G. Venanzoni, G. Addamo, F. Paonessa, and G. Virone. "3D printing of microwave and millimeter-wave filters: Additive manufacturing technologies applied in the development of high-performance filters with novel topologies." *IEEE Microwave Magazine*, 21(6), pp. 24-45, 2020. <https://doi.org/10.1109/MMM.2020.2979153>.
9. A. Tamayo-Domínguez, J.-M. Fernández-González, and M. Sierra-Pérez. "Groove gap waveguide in 3-D printed technology for low loss, weight, and cost distribution networks". *IEEE Transactions on Microwave Theory and Techniques*, 65(11), pp. 4138-4147, 2017. <https://doi.org/10.1109/TMTT.2017.2709305>.
10. B. Al-Juboori, J. Zhou, Yi Huang, M. Hussein, A. Alieldin, W. J. Otter, D. Klugmann, and S.Lucyszyn. "Lightweight and low-loss 3-D printed millimeter-wave bandpass filter based on gap-waveguide." *IEEE Access* 7. 2624-2632, 2019. <https://doi.org/10.1109/ACCESS.2018.2886210>.
11. R. Cameron, C. Kudsia, and R. Mansour, *Microwave Filters for Communication Systems*. Hoboken, NJ, USA: Wiley, 2018.
12. X. Shang, M. Lancaster, and Y. Dong, "W-band waveguide filter based on large TM_{120} resonators to ease CNC milling." *Electronic Letters*, 53(7), pp. 488-490, 2017. <https://doi.org/10.1049/el.2016.4131>.
13. C.Bartlett, and M. Höft. "W-band TE_{102} -mode filter with doubly loaded E-plane and H-plane irises". *Electronics Letters*, 57 4 190-192, 2021. <https://doi.org/10.1049/ell2.12003>.
14. A. Tamayo-Domínguez, J. -M. Fernández-González, and M. Sierra-Castañer. "3-D-printed modified butler matrix based on gap waveguide at W-Band for monopulse radar". *IEEE Transactions on Microwave Theory and Techniques*, 68(3), pp. 926-938, 2020. <https://doi.org/10.1109/TMTT.2019.2953164>.
15. A. Tamayo-Domínguez, J. -M. Fernández-González, and M. Sierra-Castañer. "Monopulse radial line slot array antenna fed by a 3-D-printed cavity-ended modified butler matrix based on gap waveguide at 94 GHz". *IEEE Transactions on Antennas and Propagation*, 69(8), pp. 4558-4568, 2021. <https://doi.org/10.1109/TAP.2021.3060045>.
16. S. B. Cohn. "Dissipation loss in multiple-coupled-resonator filters". *Proceedings of the IRE*, 1959, 47(8): 1342-1348. <https://doi.org/10.1109/JRPROC.1959.287201>.
17. J. Xu, JQ. Ding, Y. Zhao, and J. Ge. "W-Band broadband waveguide filter based on H-plane offset coupling." *Journal of Infrared, Millimeter, and Terahertz Waves* 40(2019): 412-418. <https://doi.org/10.1007/s10762-019-00571-7>.

18. B. Ahmadi, and A. Banai. "Direct coupled resonator filters realized by gap waveguide technology". IEEE Transactions on Microwave Theory and Techniques, 63(10), pp. 3445-3452, 2015. <https://doi.org/10.1109/TMTT.2015.2457916>.
19. C. Bartlett, J. Bornemann, and M. Höft. "3-D-Printing and high-precision milling of W-band filter components with admittance inverter sequences". IEEE Transactions on Components, Packaging and Manufacturing Technology, 11, pp. 2140-2147, 2021. <https://doi.org/10.1109/TCPMT.2021.3116220>.
20. X. Shang, P.Penchev, C.Guo, M.J.Lancaster, S.Dimov, Y.Dong, M.Favre, M.Billod, and E. de Rijk. "W-band waveguide filters fabricated by laser micromachining and 3-D printing". IEEE Transactions on Microwave Theory and Techniques, 64, pp. 2572-2580, 2016. <https://doi.org/10.1109/TMTT.2016.2574839>.
21. Y. Shi, J.Zhang, M. Zhou, W.Feng, B.Cao and W. Che. "Miniaturized W-band gap waveguide band-pass filter using the MEMS technique for both waveguide and surface mounted packaging". IEEE Transactions on Circuits and Systems II: Express Briefs, 66(6), pp. 938-942, 2019. <https://doi.org/10.1109/TCSII.2018.2873236>.

Publisher's Note Springer Nature remains neutral with regard to jurisdictional claims in published maps and institutional affiliations.